Periodico di Mineralogia (2011), 80, 1 (Special Issue), 57-73 DOI: 10.2451/2011PM0005

PERIODICO di MINERALOGIA
established in 1930

An International Journal of
MINERALOGY, CRYSTALLOGRAPHY, GEOCHEMISTRY, ORE DEPOSITS, PETROLOGY, VOLCANOLOGY
and applied topics on *Environment*, *Archeometry* and *Cultural Heritage*

Special Issue in memory of Sergio Lucchesi

Elbaite-liddicoatite from Black Rapids glacier, Alaska

Aaron J. Lussier[1], Frank C. Hawthorne[1,*], Vladimir K. Michaelis[2], Pedro M. Aguiar[2] and Scott Kroeker[2]

[1]Department of Geological Sciences, University of Manitoba, Winnipeg, Canada
[2]Department of Chemistry, University of Manitoba, Winnipeg, Canada
[*]Corresponding author: *frank_hawthorne@umanitoba.ca*

Abstract

Liddicoatite, ideally $Ca(AlLi_2)Al_6(SiO_6)(BO_3)_3(OH)_3F$, is an extremely rare species of tourmaline, found in very few localities worldwide. A large (~ 2 cm in cross section), euhedral sample of tourmaline retrieved from atop the Black Rapids glacier, Alaska, is shown to vary from a light pink elbaite in the core region, average composition $(Na_{0.4}Ca_{0.3}\square_{0.3})(Al_{1.75}Li_{1.25})Al_6(BO_3)_3(Si_6O_{18})F_{0.4}(OH)_{3.6}$, to a pale green liddicoatite at the edge of the crystal, $(Na_{0.3}Ca_{0.6}\square_{0.1})(Al_{1.0}Li_{1.6}Fe_{0.2}Mn_{0.2})Al_6(BO_3)_3(Si_6O_{18})F_{1.0}(OH)_{3.0}$. Detailed electron-microprobe analysis and ^{11}B and ^{27}Al Magic-Angle-Spinning Nuclear Magnetic Resonance spectroscopy show that several substitutions were active during growth, with $^{X}\square + {}^{Y}Al \rightarrow {}^{X}Ca + {}^{Y}Li$ (liddicoatite-rossmanite solid-solution) and $2{}^{Y}Al + {}^{X}\square \rightarrow 2{}^{Y}M^* + {}^{X}Ca$ accounting for most of the compositional variation. Throughout the tourmaline, there are instances of reversals in the trends of all major constituents, although few compositional gaps are observed. Most notably, a sharp decline in Ca content from ~ 0.35 to ~ 0.05 apfu (atoms per formula unit) with increasing distance from the core at ~ 2 mm from the crystal edge is followed by a sharp rise in Ca content (to 0.55 apfu), along with (Fe + Mn) content (from 0.01 to 0.35 apfu). In the core region, the origin of the Ca in the tourmaline is not clear; the correlation of Ca and F is consistent with both (1) a melt in which Ca was held as complexes with F, or (2) earlier contamination of the melt by a (Ca, F)-rich fluid. Close to the rim, a dramatic increase in Ca, F, Mn and Fe is probably due to late-stage contamination by fluids that have removed these components from adjacent wallrocks.

Key words: liddicoatite; elbaite; tourmaline; late-stage Ca enrichment; pegmatite; zoning; electron-microprobe analysis; Black Rapids glacier, Alaska; ^{11}B MAS NMR; ^{27}Al MAS NMR.

Introduction

As a result of their large stability field and extensive compositional variability, the minerals of the tourmaline group are petrogenetic indicator minerals that have been used extensively in the study of pegmatite emplacement history, fluid evolution and progressive crystallization (Novák and Povondra, 1995; Novák et al., 1999; Aurisicchio et al., 1999; Dyar et al., 1999; Selway et al., 1999; 2000a; 2000b; 2002; Tindle et al., 2002; 2005; Agrosi et al., 2006; Neiva et al., 2007; Soares et al., 2008; Zhang et al., 2008a; 2008b), and metamorphic petrology (e.g., Henry and Guidotti, 1985; Henry and Dutrow, 1992; 1996). Well-developed compositional zonation in elbaite often reflects growth in pockets of a miarolic pegmatite (London and Manning, 1995; Federico et al., 1998; London, 1999; Selway et al., 1999; 2000a; 2000b; 2002), and as such, even single crystals can provide comprehensive records of the evolution of magmatic and hydrothermal fluids (Dutrow and Henry, 2000; Lussier et al., 2008a; 2008b; 2009; 2010; 2011; Lussier and Hawthorne, 2011).

Liddicoatite, ideally $Ca(AlLi_2)Al_6(SiO_6)(BO_3)_3(OH)_3F$ (Hawthorne and Henry, 1999) is an extremely rare species of tourmaline. To date, it has been found in abundance only in Madagascar (Dunn et al., 1977; Aurisicchio et al., 1999; Akizuki et al., 2001; Dirlam et al., 2002). Other occurrences have been reported from Mozambique (Sahama et al., 1979), Malkhan, Russia (Zagorskyi et al., 1989), the Czech Republic (Novák and Povondra, 1995; Novák and Selway, 1997; Novák et al., 1999), Nigeria, Tanzania and Vietnam (Dirlam et al., 2002), southeastern Manitoba (Teertstra et al., 1999) and northeastern Ontario (Tindle et al., 2005). Examination of pink-to-green tourmaline retrieved from the Black Rapids glacier in Alaska showed it to consist primarily of elbaite with a thin rim of liddicoatite. As part of our general study on zoning in tourmaline (Lussier et al., 2008a; 2008b; 2009; 2010; 2011; Lussier and Hawthorne, 2011) we present our results on the Black Rapids tourmaline.

Sample description

The tourmaline crystal examined here was retrieved from the surface of the Black Rapids glacier in the Alaska Range, Alaska. Several prismatic crystals ranging from 0.5-1.5 x 1.0-5.0 cm were acquired, all embedded in massive quartz, and all were broken such that no terminations were present. All crystals show two pronounced colour zones: (1) pale pink, which makes up the interior of the crystal; (2) green, which makes up the outer 3-5 mm (Figure 1a, b). The largest crystal (~ 5 by 1.5 cm) was extracted for study (Figure 1b). Lussier et al. (2009) reported the $^{[4]}B$ and $^{[4]}Al$ contents of the tourmaline sample examined here, but did not give details of the spectra.

Magic-Angle-Spinning Nuclear-Magnetic-Resonance spectroscopy

The MAS NMR spectra of ^{11}B (ν_L = 192.4 MHz) and ^{27}Al (ν_L = 156.3 MHz) were recorded with a Varian ^{UNITY}Inova 600 spectrometer (14.1 T). Between 10 and 35 mg of powdered sample (~ 15 μm crystallites) was placed in a 3.2 mm (22 μL capacity) zirconia rotor and spun at 18,000-21,000 ± 5 Hz in a 3.2 mm double-resonance Varian-Chemagnetics probe. The optimized recycle delay was determined independently for each sample; averages were 90 and 12 s for ^{11}B and ^{27}Al, respectively. The final spectra are composites of 512 (^{11}B) and 512 (^{27}Al) averaged scans and were referenced to 0.1 M H_3BO_3 as a secondary reference (δ = +19.6 ppm with respect to $BF_3(CH_3CH_2)_2O$), and 1.1 M $Al(NO_3)_3$ (0.0 ppm). Pulse widths were selected to coincide approximately with a 20° tip angle at an rf nutation frequency of 50 kHz. In all parts of the Black Rapids tourmaline except

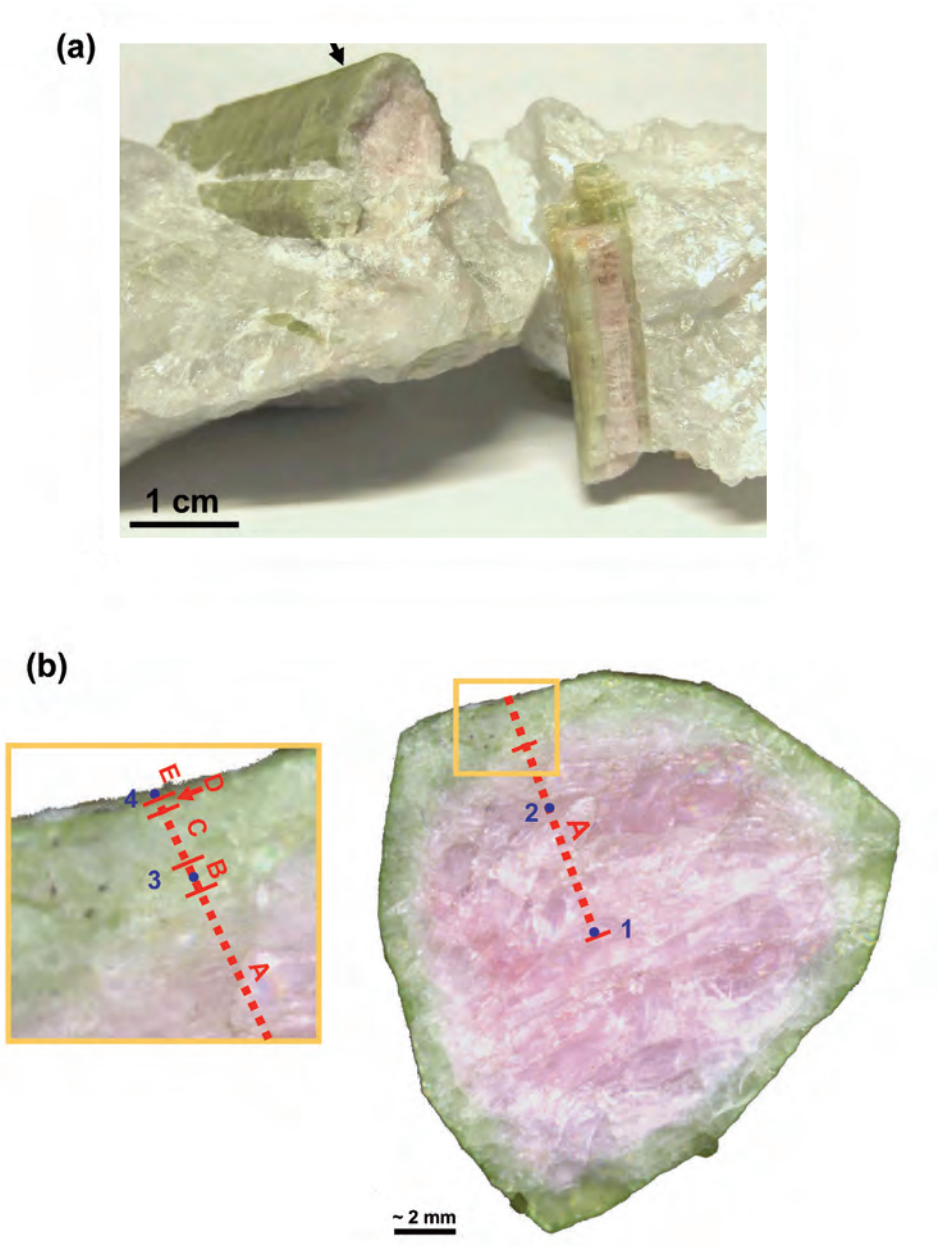

Figure 1. Sample of pink-green tourmaline retrieved from the surface of the Black Rapids glacier, Alaska. (a) the crystal embedded in quartz; the arrow indicates the approximate location of the slice take for analysis; (b) cross section used for electron-microprobe analysis. The dotted line indicates the location of the analytical traverse. Letters correspond to regions of different compositional trends (Figure 4); the numbers correspond to the positions of the compositions given in Table 1.

Table 1. The extreme liddicoatite and elbaite chemical compositions (wt%) and formulae (apfu) for Black Rapids glacier tourmaline.

	1**	2	3	4
SiO_2	37.87	37.41	37.65	37.46
TiO_2	0.00	0.00	0.01	0.04
B_2O_3*	11.38	11.61	11.24	11.19
Al_2O_3	41.21	41.99	42.19	39.02
MgO	0.00	0.01	0.00	0.04
CaO	2.15	1.71	0.40	3.29
MnO	0.09	0.06	0.15	0.54
FeO	0.00	0.01	0.32	1.89
ZnO	0.04	0.00	0.04	0.03
Li_2O*	2.32	2.08	1.84	2.26
Na_2O	1.43	1.51	1.91	1.30
K_2O	0.01	0.02	0.02	0.02
H_2O*	3.18	3.19	3.36	2.79
F	1.44	1.40	1.00	2.16
O = F	-0.61	-0.59	-0.42	-0.91
Σ	100.65	100.41	99.71	101.12
Si	5.877	5.811	5.889	5.891
B	0.048	0.113	0.035	0.037
Al	0.075	0.076	0.077	0.072
ΣT	6.000	6.000	6.000	6.000
B	3.000	3.000	3.000	3.000
Al	6.000	6.000	6.000	6.000
Al	1.536	1.688	1.777	1.233
Ti^{4+}	0.000	0.000	0.001	0.005
Mg	0.000	0.003	0.000	0.009
Fe^{2+}	0.000	0.001	0.042	0.249
Mn^{2+}	0.012	0.007	0.020	0.072
Zn^{2+}	0.005	0.000	0.005	0.003
Li	1.448	1.301	1.156	1.430
ΣY	3.000	3.000	3.000	3.000
Na	0.430	0.454	0.579	0.396
Ca	0.357	0.285	0.067	0.554
K	0.002	0.004	0.004	0.004
□	0.211	0.257	0.350	0.045
ΣX	1.000	1.000	1.000	1.000
OH	3.291	3.310	3.506	2.926
F	0.709	0.690	0.495	1.074
Σ(V + W)	4.000	4.000	4.000	4.000

* Calculated by stoichiometry

** Numbers correspond to locations marked on Figure 1b

the outermost green rim, the paramagnetic contents are quite low (Table 1) and the spectra of both ^{11}B and ^{27}Al are well-resolved over the regions of interest (Figures 2, 3).

Electron-microprobe analysis

Electron-microprobe data were collected from centre to edge on a polished slab of the large crystal, cut perpendicular to the *c*-axis, using a Cameca SX100 electron microprobe operating at 15 kV, probe current 20 nA, beam diameter 10 μm, peak count-time 20 s, background count-time 10 s. The following standards and analysing crystals were used for Kα X-ray lines: TAP: Si, diopside; Al, andalusite; Mg, forsterite; LTAP: Na, albite; F, fluororiebeckite; LPET: K, orthoclase; Ca, diopside; Ti, titanite: LLiF: Fe, fayalite; Mn, spessartine; V, V_2PO_7; Cr, chromite; Zn, gahnite.

Results

^{11}B MAS NMR spectra

All ^{11}B spectra (e.g., Figure 2) show strong

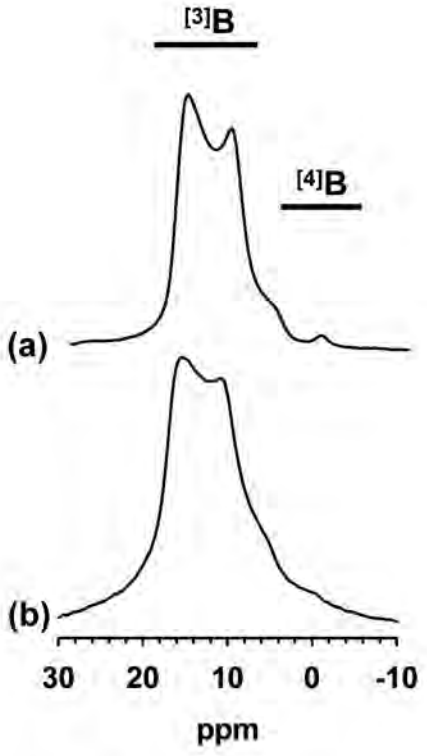

Figure 2. ^{11}B MAS NMR spectra of Black Rapids tourmaline collected on material removed from (a) pink centre of the crystal; $^{[3]}B$ simulations revealed C_Q = 2.9 ± 0.1 MHz, δ_{iso} = 18.7 ± 0.1 ppm, and η = 0.2 ± 0.05 with the fraction of $^{[4]}B$ <1%; (b) green edge of the crystal; $^{[3]}B$ simulations revealed C_Q = 2.9 ± 0.05 MHz, δ_{iso} = 18.8 ± 0.1 ppm, and η = 0.05 ± 0.05.

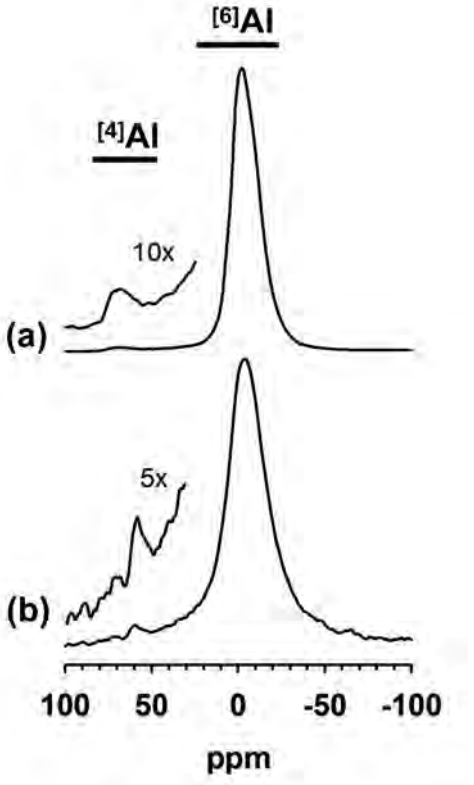

Figure 3. ^{27}Al MAS NMR spectra of Black Rapids tourmaline collected on material removed from (a) pink centre; (b) green edge. The quadrupolar couplings for ^{Y}Al site are between 3.4 and 3.6 MHz.

peaks centered at ~ 14 ppm corresponding to $^{[3]}$B (Kroeker and Stebbins, 2001), and a weak narrow peak at ~ 0 ppm, corresponding to $^{[4]}$B, where the ratio of the intensities of these signals gives the relative amounts of $^{[3]}$B and $^{[4]}$B (Bray, 1999; Michaelis et al., 2007). As the amount of $^{[3]}$B is known exactly (3.0 apfu), the amount of $^{[4]}$B may be derived. Calculation of ^{11}B MAS NMR spectra collected at 14.1 T was done using the time-domain density-matrix calculation program STARS (Skibsted et al., 1991), as implemented in the spectrometer software. Isotropic chemical shifts (δ_{iso}), quadrupole coupling constants (C_Q), and quadrupole asymmetry parameters (η) were obtained for the different B sites by manual adjustment of these parameters for all transitions, beginning with the values obtained for elbaite and liddicoatite by Tagg et al. (1999) and Lussier et al. (2008a). The average simulated parameters for $^{[3]}$B are $\delta_{iso} = 18.8 \pm 0.1$ ppm, $C_Q = 2.9 \pm 0.1$ MHz and $\eta = 0.05 \pm 0.02$. For each spectrum, the same value of the Lorentzian line-broadening (200-500 Hz) was added for both B sites in order to improve agreement between the observed and simulated spectra. Simulated values of $^{[4]}$B in Black Rapids tourmaline averaged ≤ 0.03 apfu. Intensities were converted into site populations using the expression $^{[4]}B = 3 \times {}^{[4]}I^{B} / {}^{[3]}I^{B}$ apfu (Lussier et al., 2009).

^{27}Al MAS NMR spectra

The peaks centered at ~ 0 ppm and ~ 60-70 ppm (Figure 3) correspond to $^{[6]}$Al at the *Y*- and *Z*-sites, and $^{[4]}$Al at the *T*-site in tourmaline (Lussier et al., 2009). The ^{27}Al MAS NMR spectra were modeled with asymmetric Lorentzian- Gaussian peakshapes from which the integrated intensities were determined. In all samples, $^{[4]}$Al is visible in the region 60-70 ppm (Figure 3), and the intensities were converted into site populations using the expression $^{[4]}Al = Al_{total} \times {}^{[4]}I^{Al} / ({}^{[4]}I^{Al} + {}^{[6]}I^{Al})$ apfu. The results of peak fitting indicate that < 2% of the total Al is [4]-coordinated. The quadrupolar coupling constants for $^{[6]}$Al were estimated from the breadth of the spinning side-band manifold to be of the order of 3.5 ± 0.2 MHz (Skibsted et al., 1991). For the average composition of Black Rapids tourmaline (Table 1), this corresponds to < 0.08 apfu.

Formula calculation and site occupancy

The ^{11}B and ^{27}Al magic-angle-spinning nuclear magnetic resonance (MAS NMR) spectra (Figures 2 and 3) show that both the pink core and the green rind of this crystal contain small amounts of tetrahedrally-coordinated B and Al at the *T*-site, ≤ 0.03 and < 0.08 apfu, respectively. Furthermore, the results of crystal-structure refinement of selected crystals of this sample of Black Rapids tourmaline (not presented in detail here) show <*T*-O> distances of 1.620 Å, in accord with $^{[4]}$B and $^{[4]}$Al being present (in small amounts, as indicated by the chemical analyses for SiO_2, Table 1). The tourmaline data were normalized on 31 anions with (OH) + F = 4 apfu and Li = 3 - Σ*Y*. From the spectroscopic and crystallographic results, $^{[4]}$B and $^{[4]}$Al were incorporated into the calculation in the following way for the analyses in Table 1. For each analysis, the amount of B_2O_3 was calculated by iteration such that the content of the *T* site is Si + $^{[4]}$B + $^{[4]}$Al = 6 apfu and $^{[4]}$Al is in accord with the amount of $^{[4]}$Al determined by ^{27}Al MAS NMR spectroscopy. Three of the four analyses are in accord with the amounts of $^{[4]}$B and $^{[4]}$Al determined by MAS NMR (i.e. Si ≈ 5.89 apfu); point 2 has slightly less Si and $^{[4]}$B + $^{[4]}$Al is hence slightly higher than the values indicated by MAS NMR (of different samples). For all analyses where spectroscopic and crystallographic data were not available (Figures 4-8), formulae were calculated with Si + ^{T}B + ^{T}Al = 6.000 apfu and ^{T}B = ^{T}Al.

Spatial variation in chemical composition

Figure 1b shows the location of the analytical

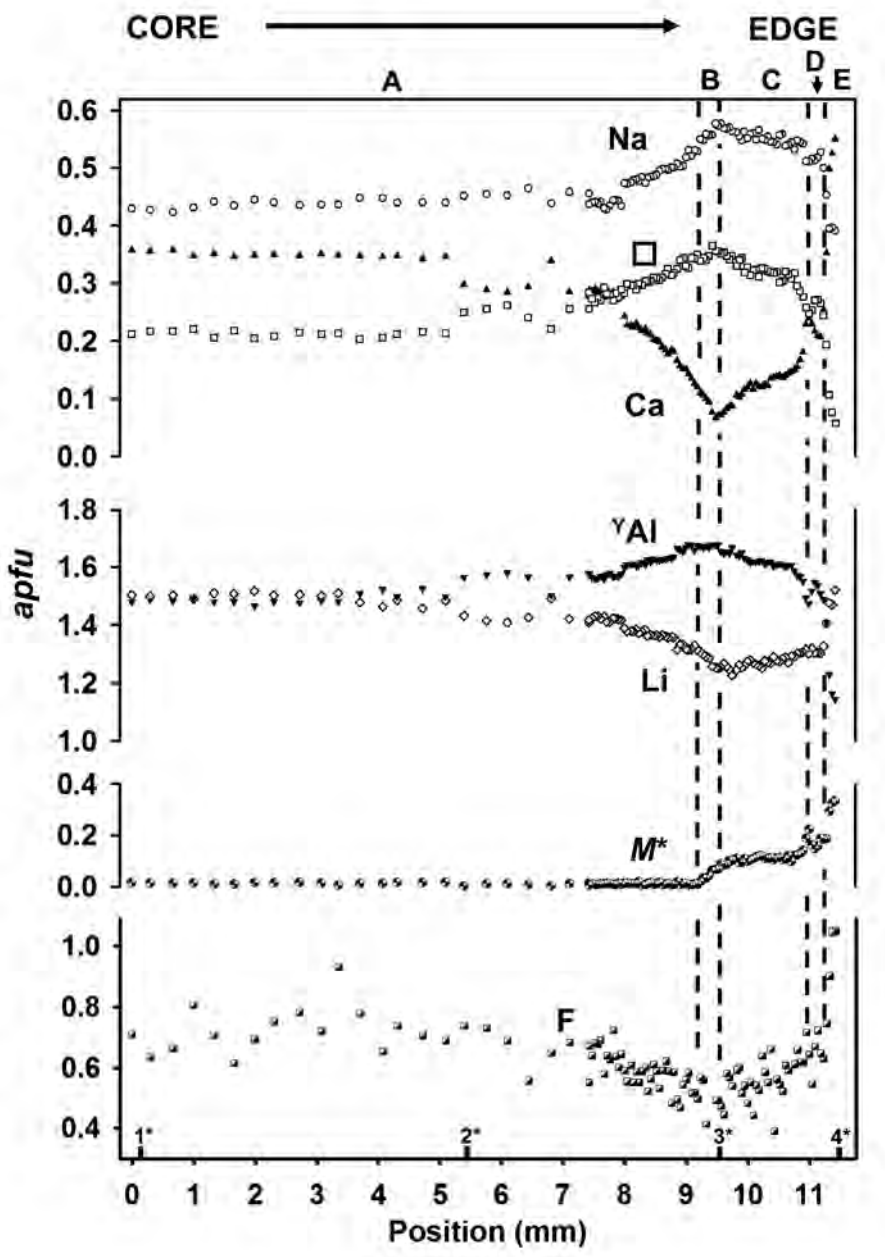

Figure 4. Variation in chemical composition of Black Rapids glacier tourmaline as a function of position along the traverse shown in Figure 1. Na (○); Vacancy (□); Ca (▲); ^{Y}Al (▼); ^{Y}Li (◇); M* (◒); F (◪). The letters A-D correspond to regions of distinct substitution behaviour. The black marks and associated numbers at the bottom of the figure indicate the location of the compositions in Table 1.

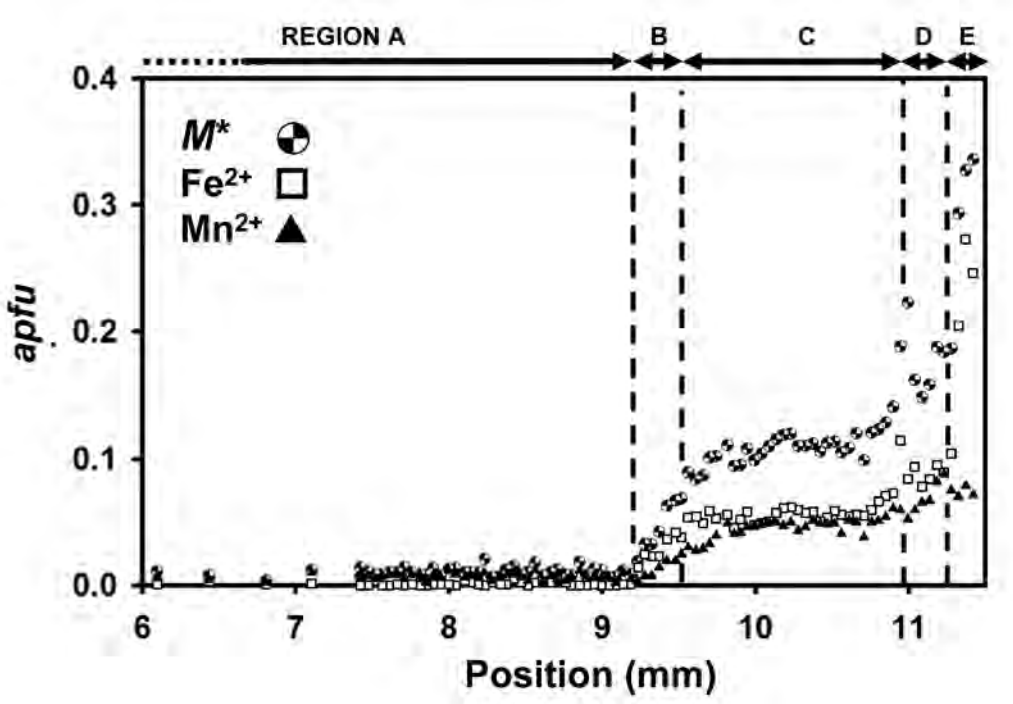

Figure 5. Variation in transition metals, M*, in the outer 6 mm of the traverse; M*(◔) is separated into its Fe^{2+} (□) and Mn^{2+} (▲) constituents.

traverse across the prism of the Black Rapids sample, and Figure 4 summarizes the variation in all major constituents as a function of position along the traverse. In the central pink region, between 0.0 and ~9.2 mm, the average sum of the transition metals, M* (= Fe^{2+} + Mn^{2+} + Ti^{4+} + Zn^{2+} + Mg) is extremely low (~ 0.01 apfu). However, (Ti^{4+} + Zn^{2+} + Mg) is close to 0.0 apfu, and the Mn^{2+} content (~ 0.01 apfu, Table 1), in the absence of any other interfering transition-element, gives rise to the pink colour of the core. For most of the pink core, the composition is essentially invariant. There is a minor discontinuity between ~ 5.1 and ~ 8.0 mm, where ^{X}□ and ^{Y}Al increase abruptly and ^{X}Ca and ^{Y}Al decrease abruptly by ~ 0.1 apfu, but Na and M* are unaffected by this change in the other constituents.

The green rind shows a far more dramatic variation in composition. Between ~8.0 and ~9.5 mm, the Na, □, and ^{Y}Al contents increase monotonically, whereas Ca, Li and F decrease monotonically. At ~ 9.2 mm, just before Ca is at a minimum, M* abruptly begins to increase. Figure 5 shows the variation of M* and its dominant constituent species Fe^{2+} and Mn^{2+} as a function of position in the outer region of the crystal. In this outer region, the Fe^{2+} content becomes greater than the Mn^{2+} content, accounting for the green colour of the rim. At 9.3 mm, the Na, □, and ^{Y}Al contents begin to decrease (Figure 4) whereas Ca, Li and F begin to increase monotonically. At ~10.8 cm, Na, □, and ^{Y}Al contents begin to decrease more rapidly whereas Ca, Li and F begin to increase more

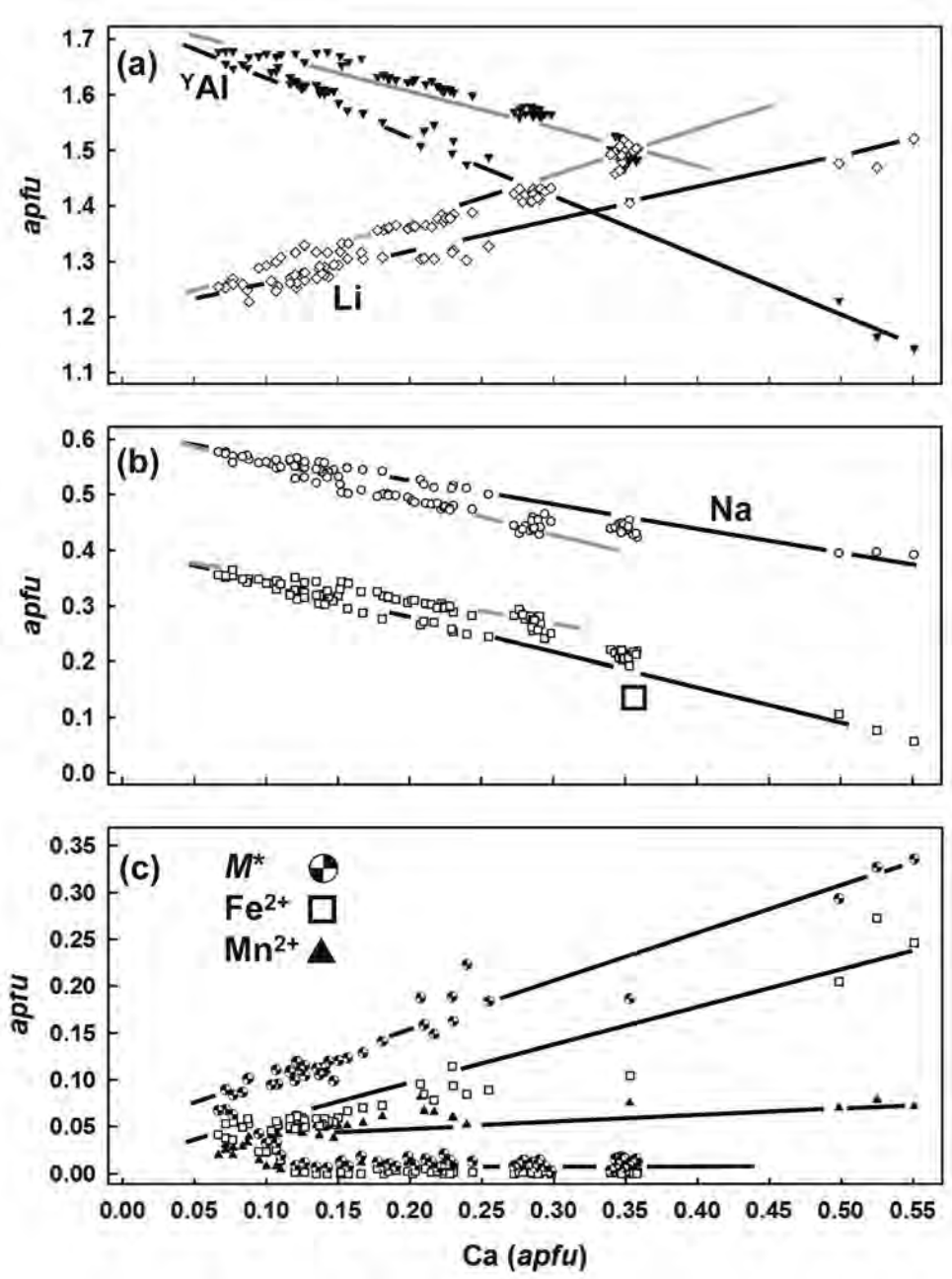

Figure 6. Variation in chemical composition of Black Rapids glacier tourmaline: (a) Al and Li as a function of Ca; (b) Na and □ (vacancy) as a function of Ca; (c) M*, Fe^{2+} and Mn^{2+} as a function of Ca. The lines are drawn as guides to the eye.

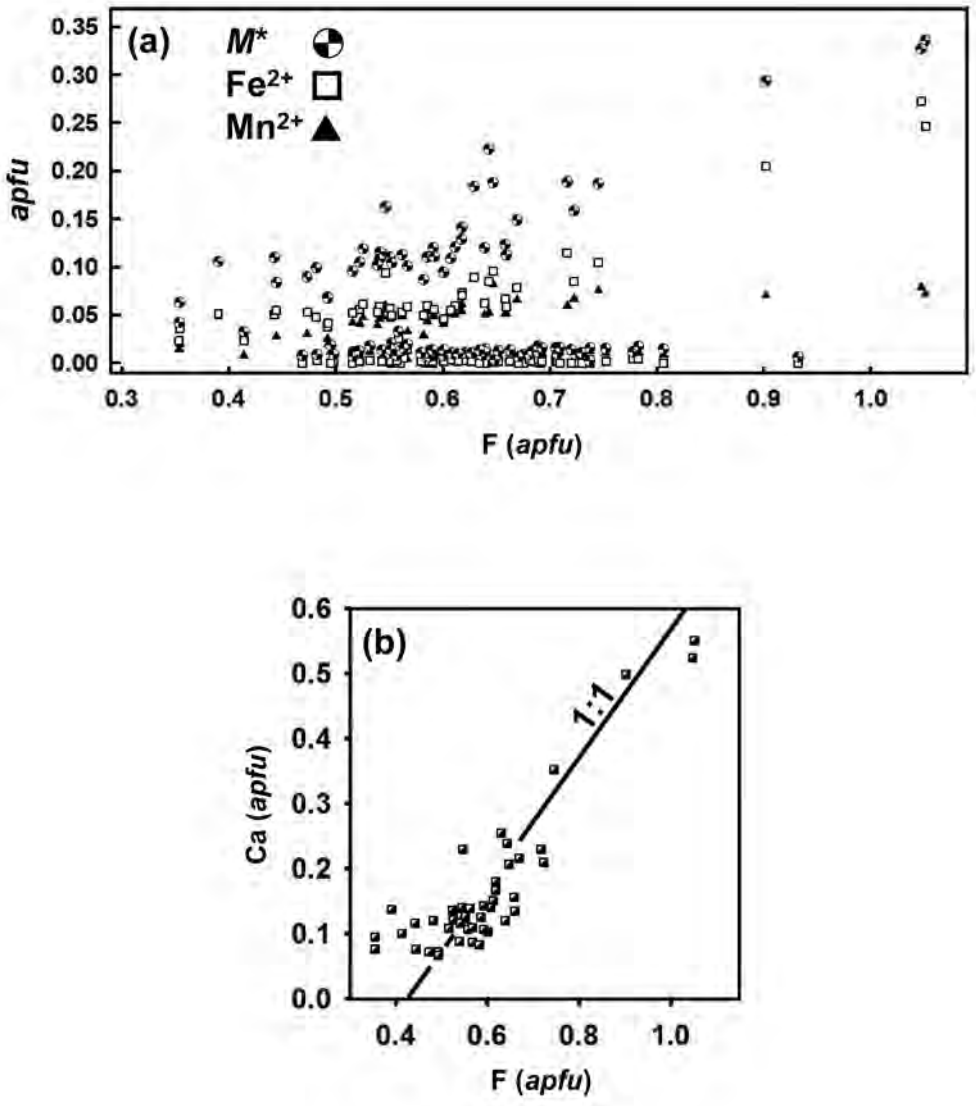

Figure 7. Variation in chemical composition of Black Rapids glacier tourmaline as a function of F: (a) M*, Fe^{2+} and Mn^{2+}; (b) Ca. The slope of the line in Figure 7b is unity.

rapidly. In the outer 0.4 mm of the crystal (~ 11.1 to ~ 11.5 mm), Ca, M* and F increase significantly, from ~ 0.20 to ~ 0.57, 0.15 to 0.35, and 0.7 to 1.0 apfu, respectively. Thus the Black Rapids glacier tourmaline is elbaite with a thin (0.2 mm) rind of liddicoatite. On the basis of spatial chemical variation, we may divide the crystal into five distinct regions, marked A-E in Figures 1, 4 and 5.

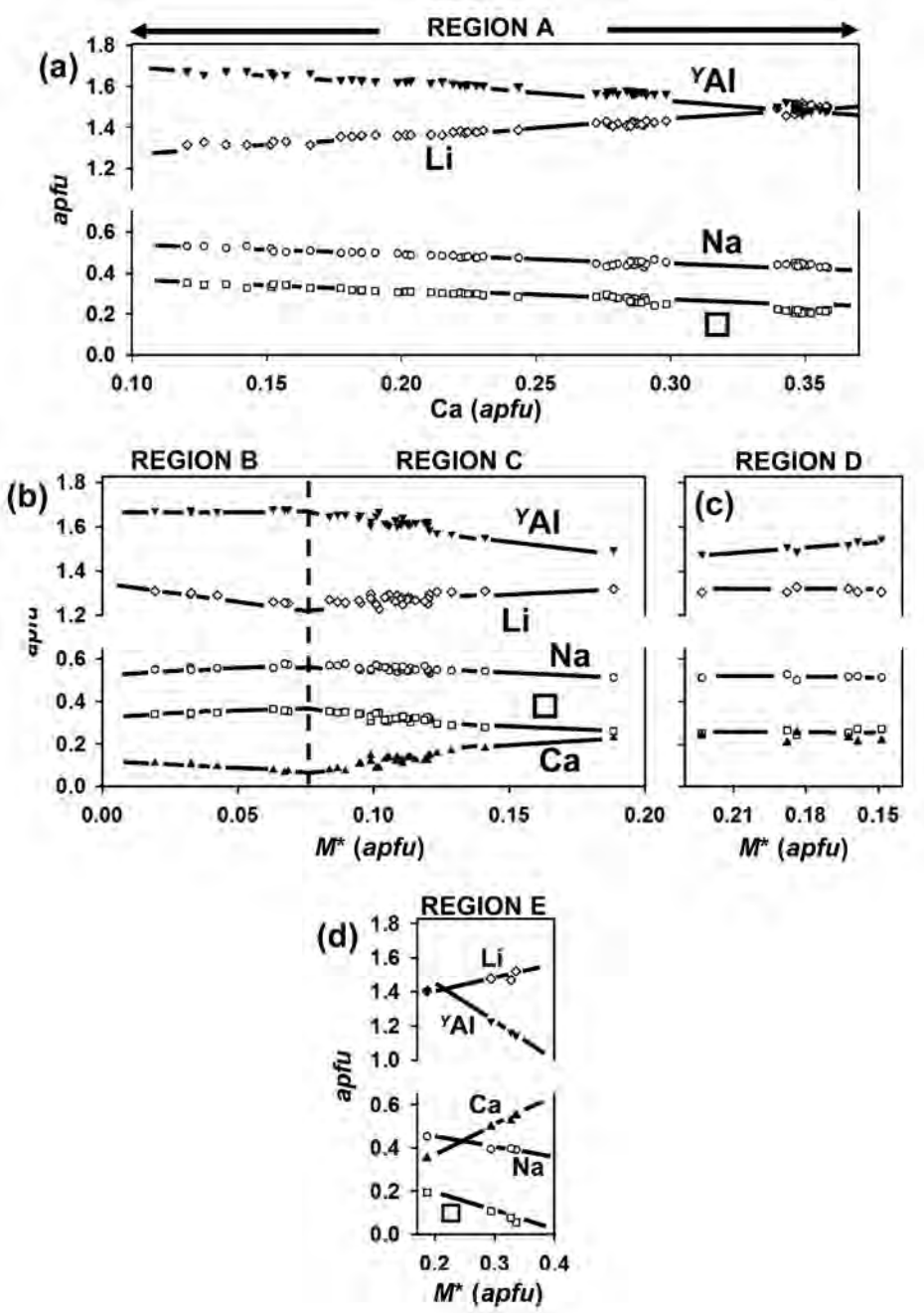

Figure 8. Variation in composition of Black Rapids glacier tourmaline: (a) Al, Li, Na, and □ versus Ca for region A; (b-d) Li, ^{Y}Al, Na, Ca and □ versus M* for regions B, C, D and E. The lines are drawn as guides to the eye.

Bulk chemical variation: from elbaite to liddicoatite

The total chemical variation in the crystal is shown in Figure 6 as a function of Ca content, and ranges from elbaite, $Na_{0.58}Ca_{0.07}\square_{0.35}[Li_{1.27}Al_{1.66}M^*_{0.07}]Al_6[Si_{5.89}B_{0.03}Al_{0.08}]O_{18}(BO_3)_3(OH)_{3.53}F_{0.47}$, to liddicoatite, $Na_{0.39}Ca_{0.55}\square_{0.06}[Li_{1.52}Al_{1.14}M^*_{0.34}]Al_6[Si_{5.89}B_{0.03}Al_{0.08}]O_{18}(BO_3)_3(OH)_{2.95}F_{1.05}$. There are two distinct trends in Figure 6 that we can understand from inspection of Figure 4. In region A of the crystal, the amount of the M* component is ~ 0.01 apfu, whereas in regions B-E, the amount of M* increases toward the edge of the crystal. Thus in regions B-E, the greater amount of M* results in a lower content of ^{Y}(Al + Li), resulting in the compositional trend indicated by the black lines in Figure 6a and b. In region A, the lower content of M* results in the compositional trend with higher amounts of Al and Li indicated by the grey lines in Figure 6a and b. The presence of two trends and the role of M* is confirmed by the variation of M* (and its various constituents) as a function of Ca (Figure 6c). It should be emphasized that Figure 6 gives only the chemical variations in the tourmaline and contains no information concerning the spatial aspects of zoning. However, the presence of two distinct trends in compositional change indicates that crystallization has not proceeded to completion by simple crystallization from an initial melt or fluid. There has been a hiatus in crystallization, and the presence of two distinct trends suggests a contamination event whereby the crystallizing melt or fluid has been contaminated by an external fluid of distinctly different composition.

Correlations as a function of F content are shown in Figure 7. There is a lot of scatter in these trends because of the scatter in the F values; nevertheless, two important issues are apparent. First, the variation in M*, Fe^{2+} and Mn^{2+} shows two distinct trends (Figure 7a), one with M*, Fe^{2+} and Mn^{2+} close to 0 apfu (and corresponding to region A of the crystal), and one with M*, Fe^{2+} and Mn^{2+} increasing with increasing Ca in regions B-E. There is also a strong 1:1 correlation between Ca and F (except for the lowest values of F, Figure 7b), and inspection of Figure 4 shows that Ca and F track each other through some fairly dramatic changes in behaviour as a function of position in the crystal. The F content reaches a maximum of 1 apfu at the edge of the crystal, corresponding to the highest liddicoatite content of the crystal.

Substitution mechanisms in Black Rapids tourmaline

For the entire pink central region of the crystal (from 0 to 9.1 mm; region A, Figure 4), the observed substitutions are as follows (Figure 8a):

$$(1) \quad {}^X\square + {}^Y\mathrm{Al} \rightarrow {}^X\mathrm{Ca} + {}^Y\mathrm{Li} \qquad (0.13)$$
$$(2) \quad {}^X\mathrm{Ca}_2 + {}^Y\mathrm{Li} \rightarrow {}^X\mathrm{Na}_2 + {}^Y\mathrm{Al} \qquad (0.06)$$

where the arrows indicate replacement of ^{X}Ca and ^{Y}Li by $^X\square$, ^{Y}Al and ^{X}Na with increasing distance from the centre of the crystal from 0 to 9.1 mm. Substitution (1) describes the compositional change along the rossmanite-liddicoatite series, and substitution (2) describes the compositional change along the elbaite-liddicoatite series. The straight lines in Figure 8a show the aggregate variations represented by these substitutions. From the onset of enrichment in M* (9.2 mm; region B; Figure 4) until the minimum Ca value (9.5 mm; region B; Figure 4), the Al content of the crystal remains invariant, and the substitution mechanisms in operation are as follows (Figure 8b):

$$(3) \quad {}^X\mathrm{Na} + {}^Y\mathrm{M}^* \rightarrow {}^X\mathrm{Ca} + {}^Y\mathrm{Li} \qquad (0.04)$$
$$(4) \quad {}^X\square + {}^Y\mathrm{M}^*_3 \rightarrow {}^X\mathrm{Ca} + {}^Y\mathrm{Li}_3 \qquad (0.01)$$

At 9.2 to 9.4 mm along the traverse, the compositional profile shows a clear change where the trends of all constituents reverse

(Figures 4, 5 and 8). From 9.4 to ~ 10.9 mm (Figure 8b, region C), the inverse of substitution (1) becomes active, and the remaining chemical variation occurs *via* substitution (5):

$$(-1) \quad {}^{X}Ca + {}^{Y}Li \rightarrow {}^{X}\square + {}^{Y}Al \qquad (0.08)$$
$$(5) \quad {}^{X}Ca + {}^{Y}M^{*} \rightarrow {}^{X}Na + {}^{Y}Al \qquad (0.08)$$
$$(6) \quad {}^{X}Ca + {}^{Y}M^{*}_{2} \rightarrow {}^{X}\square + {}^{Y}Al_{2} \qquad (0.01)$$

At ~ 10.9 mm (until ~ 11.1 mm, Figures 4, 5 and 8c, region D), there is another reversal of compositional trends involving the following substitutions (Figure 8c; note reversed M* scale):

$$(7) \quad {}^{X}\square + {}^{Y}Al_{2} \rightarrow {}^{X}Ca + {}^{Y}M^{*}_{2} \qquad (0.05)$$

In the last ~ 0.2 mm of the crystal (Figures 4, 5 and 8d; region E), the trend of increasing Ca resumes and substitutions (5) and (-1) again become active together with substitution (8):

$$(-1) \quad {}^{X}Ca + {}^{Y}Li \rightarrow {}^{X}\square + {}^{Y}Al \qquad (0.12)$$
$$(5) \quad {}^{X}Ca + {}^{Y}M^{*} \rightarrow {}^{X}Na + {}^{Y}Al \qquad (0.08)$$
$$(7) \quad {}^{X}Ca + {}^{Y}M^{*}_{2} \rightarrow {}^{X}\square + {}^{Y}Al_{2} \qquad (0.05)$$

The elbaite-liddicoatite substitution (substitution 4) is relatively minor, occurring only in region B, whereas the liddicoatite-rossmanite substitution (substitution 1) accounts for the majority of the chemical variability observed.

We have disregarded possible variations in the small amount of tetrahedrally-coordinated Al and B in this sample (Figures 2, 3). The overall low amounts ($^{[4]}B + {}^{[4]}Al < 0.11$ apfu) observed in all regions of the crystal indicate that although substitution mechanisms accommodating the exchange of these constituents may be active, they are not responsible for a significant part of the compositional variation observed throughout the sample. In detailed studies of substitution mechanisms operating in elbaite and olenite tourmalines where significant amounts of $^{[4]}B$ are present, Kalt et al. (2001) and Lussier et al. (2008a) note that ${}^{T}B + {}^{Y}Al \rightarrow Si + {}^{Y}M^{*}$ is the principal mechanism accounting for variability in ${}^{T}B$. Given the composition of the Black Rapids sample, it is probable that this mechanism is in operation, although its magnitude would likely be less than 0.11 apfu in magnitude throughout the crystal.

Liddicoatite in granitic pegmatites

The scarcity of liddicoatite in granitic pegmatites is related to the unusual conditions required to concentrate substantial amounts of Ca and Li in the consolidating melt. In the typical crystallization sequence observed in granitic pegmatites, the bulk of Ca enters early-stage minerals, and is found in the endocontact and border- and wall-zone assemblages (*e.g.*, feldspar, fluorapatite). In contrast, Li is concentrated in relatively late-crystallizing phases such as Li-aluminosilicates (spodumene or petalite) and lepidolite (e.g., Černý, 1991; London, 1992). Two mechanisms have been invoked to explain the presence of Ca in late-stage minerals in granitic pegmatites. (1) Weidner and Martin (1987) proposed that F in a granitic melt may complex with Ca, and as a result, Ca can remain in the melt until late in the fractionation process. This suggestion has been adopted by several authors in the past 10 years. Selway et al. (2000a, 2002) suggested this mechanism for the crystallization of Ca-rich tourmaline as a late-stage mineral in the Tanco and Nyköpingsgruvan granitic pegmatites. The occurrence of liddicoatite in the elbaite-subtype Bližná pegmatite in the Czech Republic is argued by Novák et al. (1999) to have resulted from the crystallization of a (Na, Al, Li, B)-rich melt, wherein Ca was conserved throughout fractionation of a melt of unique composition. A similar argument is put forth to explain the occurrence of tourmaline crystals with an elbaite (Ca ~ 0.15 apfu) core and a liddicoatite (Ca ~ 0.50 apfu) rim in the High

Grade Dike, eastern Manitoba, Canada. Here, Teertstra et al. (1999) observe no evidence of a potential secondary source of Ca. In both of these occurrences, F- and Ca-contents are positively correlated in the tourmaline, consistent with the development of Ca-F complexes that delay the onset of Ca precipitation. (2) Calcium may be introduced into the pegmatite system at any stage as a contaminant. Thus in the McCombe pegmatite of northwestern Ontario, Canada (Tindle et al., 2005), the precipitation of Ca-rich elbaite is argued to be the result of assimilation and leaching of Ca, Mg, and Ti from the host rock and introduction into late-stage pegmatite melt or fluid. With this particular mechanism, one does not expect just an increase of Ca and F, but a change in other constituents that have been involved in the contamination process.

Zoning in Black Rapids tourmaline

In Black Rapids tourmaline, the lack of transition metals in the central core-zone A indicates that the pegmatite melt had fractionated sufficiently to remove all transition metals from the melt. This situation is in accord with the occurrence of this tourmaline in massive quartz that is presumably part of the quartz core of the parent pegmatite. Despite this indication of a highly fractionated parent melt, the core of the tourmaline has approximately 0.35 apfu Ca and 0.75 apfu F which is uniform across ~ 7 mm of the pink core. So what is the source of this Ca and F? The only other constituents of the core of the tourmaline are H, Li, B, Na, Al and Si, all common constituents of a highly fractionated granitic melt. The "foreign constituents" are Ca and F, suggesting either (1) they have come from a Ca-F fluid introduced in a prior contamination event, or (2) the Ca and F come from primary Ca-F complexes in the granitic melt. Toward the edge of the pink core, both Ca and F increase sharply, suggesting that both are being depleted in the nascent melt/fluid relative to the other constituents.

At the margin between the pink core and the green rim (region B, Figures 1, 4), there is a sharp change in composition: Ca, F, Li and transition metals increase, and Na and Al decrease. The Ca-F association continues, but is accompanied by the increase in Fe and Mn. It is difficult to see this as anything but a contamination event with the introduction of Ca, Fe, Mn and F, presumably the result of low-temperature hydrothermal fluids that have reacted with host-rock ferromagnesian minerals. However, Ca, Fe, Mn and F continue to rise from the junction of the pink core and green rim continuously to the edge of the crystal while Na and Al continue to fall. This change does not accord with the usual depletion of Fe and Mn with continued crystallization of tourmaline (Lussier et al., 2008b; 2010), suggesting that the contamination event may have been a continuing process until the cessation of crystallization of the tourmaline.

Conclusions

It is apparent that the spatial distribution of chemical variations in tourmaline carries a lot of information concerning the crystallization history of the tourmaline, and potentially of parts of the host pegmatite. Of particular significance is the role of Ca and F in the petrology of granitic pegmatites. Correlation between F and both Na (e.g., Selway et al., 1999; 2000a) and Ca (e.g., Novák et al., 1999) will be affected by the stereochemistry of the interaction between the *X*-site cation and the anion at the O(1) site (OH vs. F), and by various possible petrogenetic interactions between Ca and F, and both aspects of this issue still remain to be clarified in detail.

Acknowledgements

We are grateful to The Miner's Lunchbox for donating the tourmaline sample used in this work. Funding for this work was provided by a University of Manitoba Graduate Fellowship and an NSERC

PGSD to AJL and VKM, and by a Canada Research Chair in Crystallography and Mineralogy, and Discovery, Research Tools and Equipment, and Major Facilities Access grants to FCH and SK from the Natural Sciences and Engineering Research Council of Canada, and by Canada Foundation for Innovation Grants to FCH and SK.

References

Agrosi G., Bosi F., Lucchesi S., Melchiorre G. and Scandale E. (2006) - Mn-tourmaline crystals from island of Elba (Italy): growth history and growth marks. *American Mineralogist*, 91, 944-952.

Akizuki M., Kuribayashi T., Nagase T. and Kitikaze A. (2001) - Triclinic liddicoatite and elbaite in growth sectors of tourmaline from Madagascar. *American Mineralogist*, 86, 364-369.

Aurissicchio C., Demartin F., Ottolini L. and Pezzotta F. (1999) - Homogeneous liddicoatite from Madagascar: a possible reference material? First EMPA, SIMS, and SREF data. *European Journal of Mineralogy*, 11, 263-280.

Bray P.J. (1999) - NMR and NQR studies of boron in vitreous and crystalline borates. *Inorganica Chimica Acta*, 289, 158-173.

Černý P. (1991) - Rare-element granitic pegmatites, I. Anatomy and internal evolution of pegmatite deposits. *Geoscience Canada*, 18, 49-67.

Dirlam D.M., Laurs B.M., Pezzotta F. and Simmons W.B. (2002) - Liddicoatite tourmaline from Anjanabonoina, Madagascar. *Gems and Gemology*, 38, 28-53.

Dunn P.J., Appleman D.E. and Nelen J.E. (1977) - Liddicoatite, a new calcium end-member of the tourmaline group. *American Mineralogist*, 62, 1121-1124.

Dutrow B.L. and Henry D.J. (2000) - Complexly zoned fibrous tourmaline, Cruzeiro Mine, Minas Gerais, Brazil: a record of evolving magmatic and hydrothermal fluids. *Canadian Mineralogist*, 38, 131-143.

Dyar M.D., Guidotti C.V., Core D.P., Wearn K.M., Wise M.A., Francis C.A., Johnson K., Brady J.B, Robertson J.D. and Cross L.R. (1999) - Stable isotope and crystal chemistry of tourmaline across pegmatite - country rock boundaries at Black Mountain and Mount Mica, southwestern Maine, U.S.A. *European Journal of Mineralogy*, 11, 281-294.

Federico M., Andreozzi G.B., Lucchesi S. and Graziani G. (1998) - Compositional variation of tourmaline in the granitic pegmatite dykes of the Cruzeiro mine, Minas Gerais, Brazil. *Canadian Mineralogist*, 36, 415-431.

Hawthorne F.C. and Henry D.J. (1999) - Classification of minerals of the tourmaline group. *European Journal of Mineralogy*, 11, 201-215.

Henry D.J. and Dutrow B.L. (1992) - Tourmaline in low-grade clastic sedimentary rocks: and example of the petrogenetic potential of tourmaline. *Contributions to Mineralogy and Petrology*, 112, 203-218.

Henry D.J. and Dutrow B.L. (1996) - Metamorphic tourmaline and its petrogenetic applications. In Boron: Mineralogy Petrology, and Geochemistry (Grew E. and Anovitz L.M., Eds.), *Reviews in Mineralogy*, 33, Mineralogical Society of America, Washington DC, 503-557.

Henry D.J. and Guidotti C.V. (1985) - Tourmaline as a petrogenetic indicator mineral: an example from the staurolite-grade metapelites of NW Maine. *American Mineralogist*, 70, 1-15.

Kalt A., Schreyer W., Ludwig T., Prowatke S., Berhardt H.-J. and Ertl A. (2001) - Complete solid solution between magnesian schorl and lithian excess-boron olenite in a pegmatite from the Koralpe (eastern Alps, Austria). *European Journal of Mineralogy*, 13, 1191-1205.

Kroeker S. and Stebbins J.F. (2001) - Three-coordinated boron-11 chemical shifts in borates. *Inorganic Chemistry*, 40, 6239-6246.

London D. (1992) - The application of experimental petrology to the genesis and crystallization of granitic pegmatites. *Canadian Mineralogist*, 30, 499-540.

London D. (1999) - Stability of tourmaline in peraluminous granite systems: the boron cycle from anatexis to hydrothermal aureoles. *European Journal of Mineralogy*, 11, 253-262.

London D. and Manning D.A.C. (1995) - Chemical variation and significance of tourmaline from Southwest England. *Economic Geology*, 90, 495-519.

Lussier A.J. and Hawthorne F.C. (2011) - Oscillatory zoned liddicoatite from Anjanabonoina, central Madagascar. II. Compositional variations and substitution mechanisms. *Canadian Mineralogist*, 49, 89-104.

Lussier A.J., Aguiar P.M., Michaelis V.K., Kroeker S., Herwig S., Abdu Y. and Hawthorne F.C. (2008a) - Mushroom elbaite from the Kat Chay mine, Momeik, near Mogok, Myanmar: I. Crystal chemistry by SREF, EMPA, MAS NMR and Mössbauer spectroscopy. *Mineralogical Magazine*, 72, 747-761.

Lussier A.J., Hawthorne F.C., Herwig S., Abdu Y., Aguiar P.M., Michaelis V.K. and Kroeker S. (2008b) - Mushroom elbaite from the Kat Chay mine, Momeik, near Mogok, Myanmar: II. Zoning and crystal growth. *Mineralogical Magazine*, 72, 999-1010.

Lussier A.J., Aguiar P.M., Michaelis V.K., Kroeker S. and Hawthorne F.C. (2009) - The occurrence of tetrahedrally coordinated Al and B in tourmaline: A ^{11}B and ^{27}Al MAS NMR study. *American Mineralogist*, 94, 785-792.

Lussier A.J., Hawthorne F.C., Abdu Y., Herwig S., Michaelis V.K., Aguiar P.M. and Kroeker S. (2010) - The crystal chemistry of wheatsheaf tourmaline from Mogok, Myanmar. *Mineralogical Magazine*, 75 (in press).

Lussier A.J., Abdu Y., Hawthorne F.C., Michaelis V.K., Aguiar P.M. and Kroeker S. (2011) - Oscillatory zoned elbaite-liddicoatite from Anjanabonoina, central Madagascar. I. Crystal chemistry and structure by SREF and ^{11}B and ^{27}Al MAS NMR spectroscopy. *Canadian Mineralogist*, 49, 63-88.

Michaelis V.K., Aguiar P.M. and Kroeker S. (2007) - Probing alkali coordination environments in alkali borate glasses by multinuclear magnetic resonance. *Journal of Non-Crystalline Solids*, 353, 2582-2590.

Neiva A.M.R., Manuela M., Silva V.G. and Gomes M.E. (2007) - Crystal chemistry of tourmaline from Bariscan granites, associated tin-tungsten and gold deposits, and associated metamorphic and metasomatic rocks from northern Portugal. *Neues Jahrbuch für Mineralogie - Abhandlungen*, 184, 45-76.

Novák M. and Povondra P. (1995) - Elbaite pegmatites in the Moldanubicum: a new subtype of rare-element class. *Mineralogy and Petrology*, 55, 159-176.

Novák M. and Selway J.B. (1997) - Tourmaline composition as a recorder of crystallization in open and closed systems in the elbaite-subtype pegmatite at Blizná, southern Bohemia, Czech Republic. In: "Tourmaline 1997 Symposium" (Nové Mesto na Morave), Abstract Volume, 62-63.

Novák M., Selway J.B., Černý P., Hawthorne F.C. and Ottolini L. (1999) - Tourmaline of the elbaite-dravite series from an elbaite-subtype pegmatite at Blizná, southern Bohemia, Czech Republic. *European Journal of Mineralogy*, 11, 557-568.

Sahama T.G., Von Knorring O. and Törnroos R. (1979) - On tourmaline. *Lithos*, 12, 109-114.

Selway J.B., Novák M., Černý P. and Hawthorne F.C. (1999) - Compositional evolution of tourmaline in lepidolite-subtype pegmatites. *European Journal of Mineralogy*, 11, 569-584.

Selway J.B., Černý P., Hawthorne F.C. and Novák M. (2000a) - The Tanco Pegmatite at Bernic Lake, Manitoba. XIV. Internal tourmaline. *Canadian Mineralogist*, 38, 877-891.

Selway J.B., Novák M., Černý P. and Hawthorne F.C. (2000b) - The Tanco Pegmatite at Bernic Lake, Manitoba. XIII. Exocontact tourmaline. *Canadian Mineralogist*, 38, 869-876.

Selway J.B., Smeds. S-A., Černý P. and Hawthorne F.C. (2002) - Compositional evolution of tourmaline in the petalite-subtype Nyköpingsgruvan pegmatites, Utö, Stokholm Archipelago, Sweden. *GFF*, 124, 93-102.

Skibsted J., Nielsen N.C., Bildsøe H. and Jakobsen H.J. (1991) - Satellite transitions in MAS NMR spectra of quadrupolar nuclei. *Journal of Magnetic Resonance*, 95, 88-117.

Soares D.R., Beurlen H., Barreto S.D., Da Silva M.R.R. and Ferreira C.M. (2008) - Compositional variation of tourmaline-group minerals in the Borborema pegmatite province, Northeastern Brazil. *Canadian Mineralogist*, 46, 1097-1116.

Tagg S.L., Cho H., Dyar M.D. and Grew E. (1999) - Tetrahedral boron in naturally occurring tourmaline. *American Mineralogist*, 84, 1451-1455.

Teertstra D.K., Černý P. and Ottolini L. (1999) - Stranger in paradise; liddicoatite from the high Grade Dike pegmatite, southeastern Manitoba, Canada. *European Journal of Mineralogy*, 11, 227-235.

Tindle A.G., Breaks F.W. and Selway J.B. (2002) - Tourmaline in petalite-subtype granitic pegmatites: evidence of fractionation and contamination from the Pakeagama Lake and Separation Lake areas of Northwestern Ontario, Canada. *Canadian Mineralogist*, 40, 753-788.

Tindle A.G., Selway J.B. and Breaks F. (2005) - Liddicoatite and associated species from the McCombe spodumene-subtype rare-element granitic pegmatite, northwestern Ontario, Canada. *Canadian Mineralogist*, 43, 769-793.

Weidner J.R. and Martin R.F. (1987) - Phase equilibria of a fluorine-rich leucogranite from the St. Austell pluton, Cornwall. *Geochimica Cosmochimica Acta*, 51, 1591-1597.

Zagorskyi V.E., Peretyazhko I.S., Schiryevna V.A. and Bogdanova L.A. (1989) - Tourmaline from miarolitic pegmatites in the Malkhan Range (Transbaiikaia). *Mineral Zhurnal*, 11, 44-55 (in Russian).

Zhang A.C., Wang R.C., Jiang S.Y., Hu H. and Zhang H. (2008a) - Chemical and textural features of tourmaline from the spodumene-subtype Koktokay No. 3 pegmatite, Altai, Northwestern China: a record of magmatic to hydrothermal evolution. *Canadian Mineralogist*, 46, 51-58.

Zhang A.C., Wang R.C., Li Y., Hu H., Lu X., Ji J. and Zhang H. (2008b) - Tourmalines from the Koktokay No. 3 pegmatite, Altai, NW China: spectroscopy characterization and relationship with the pegmatite evolution. *European Journal of Mineralogy*, 20, 143-154.

Submitted, October 2010 - Accepted, January 2011